Optics Communications 448 (2019) 82–88

Contents lists available at ScienceDirect

Optics Communications

journal homepage: www.elsevier.com/locate/optcom

Upconversion properties of erbium nanoparticles doped tellurite glasses for high efficient laser glass

M.N. Azlan [a,b,*], M.K. Halimah [c], A.B. Suriani [a,b], Y. Azlina [a,b], S.A. Umar [d], R. El-Mallawany [e]

[a] Physics Department, Universiti Pendidikan Sultan Idris, 35900 Tanjung Malim, Perak, Malaysia
[b] Nanotechnology Research Center, Faculty of Science and Mathematics, Universiti Pendidikan Sultan Idris, 35900 Tanjung Malim, Perak, Malaysia
[c] Physics Department, Universiti Putra Malaysia, 35900, Serdang, Selangor, Malaysia
[d] Department of Physics, Faculty of Science, Bauchi State University Gadau, Nigeria
[e] Physics Department, Faculty of Science, Menoufia University, Egypt

ARTICLE INFO

Keywords:
Tellurite glass
Erbium nanoparticles
Laser glass

ABSTRACT

Erbium nano particles (NPs) doped tellurite glasses were prepared via melt-quenched technique and their chemical composition are as follows; $\{[(TeO_2)_{0.70}(B_2O_3)_{0.30}]_{0.7}(ZnO)_{0.3}\}_y$ $(Er_2O_3NPs)_{1-y}$, y = 0.005, 0.01, 0.02, 0.03, 0.04 and 0.05. The amorphous state of the glass system was revealed and the structural parameters indicating the formation of non-bridging oxygen was shown. The current work underlines the spectral parameters from Judd–Ofelt (JO) studies, and upconversion spectra. The existence of erbium NPs was found experimentally using transmission electron microscopy (TEM). The Judd–Ofelt analysis suggests that the radiative probability, A_{rad} is strong at $^2H_{11/2} \rightarrow {}^4I_{15/2}$ and a longer lifetime at $^4I_{11/2} \rightarrow {}^4I_{15/2}$. The Argon laser beam was used to determine the upconversion emission peaks. The upconversion radiation emission excited at 800 nm was found in the range 390 nm.

1. Introduction

The extensive research on glass science and technology that explore the new findings on photonic and optical applications is undeniable. The novel findings on glass applications are reported continuously [1, 2]. The high demand on communication system increase the development of potential glass materials for optical communications. There are various kind of glass materials which are beneficial for optical applications. The silicate glass is currently used as the main core in fiber optics. Besides that, silicate glass has high melting point, weak absorbance, and weak nonlinearity [3]. Research on alternative materials with high optical performance and stability are essential to replace the current optical materials. Besides that, the previous research on tellurite glasses found that there are extensive of optical applications such as yellowish green optical devices, laser applications, visible upconverter and tunable display devises [4–7]. The tellurite glass appears to be one of the unique and high demand materials for their interesting physical properties [8–13]. The tellurite glass had been widely developed in several optical applications such as fiber optics, optoelectronics, light emitting diode (LED), and glass sensors [14]. Moreover, the improvement of tellurite glass in optical applications is still in progress. The tellurite glass is compatible with many oxides materials especially lanthanide oxides. Various oxides are required to be added in tellurite glass network to improve their stability and optical properties.

Rare earth oxides are used to enhance the optical communication, and one of the applications is Er^{3+}-doped fiber amplifier (EDFA) device. Erbium oxide had been widely investigated to enhance the optical properties of tellurite glass [15]. Meanwhile, there are few information on optical performance of erbium NPs doped tellurite glass. It was reported that the size of particles affects greatly on optical performance of laser glass [16]. Metallic nanoparticles are commonly used to enhance the optical efficiency of laser glass. However, there is still much controversy about the metallic nanoparticles which is due to the degradation of emission effect on lanthanide oxide by the metallic materials. Thus, the lanthanide oxide nanoparticles are alternative materials to enhance the optical performance of laser glass. Further investigations on optical performance of erbium NPs doped tellurite glass are essential to design the photonic materials, which are accessible and understandable. The aims of this research are to determine the Judd–Ofelt parameters, emission lifetime and upconversion of erbium NPs doped tellurite glass.

2. Experimental setup

The erbium NPs doped tellurite glasses were prepared via melt-quenched technique and their chemical composition are as follows;

* Corresponding author at: Physics Department, Universiti Pendidikan Sultan Idris, 35900 Tanjung Malim, Perak, Malaysia.
E-mail addresses: azlanmn@fsmt.upsi.edu.my (M.N. Azlan), halimahmk@upm.edu.my (M.K. Halimah), suriani@fsmt.upsi.edu.my (A.B. Suriani), azlinayahya15@gmail.com (Y. Azlina), usaltilde@yahoo.com (S.A. Umar), raoufelmallawany@yahoo.com (R. El-Mallawany).

https://doi.org/10.1016/j.optcom.2019.05.022
Received 12 February 2019; Received in revised form 11 April 2019; Accepted 12 May 2019
Available online 15 May 2019

$\{[(TeO_2)_{0.70}(B_2O_3)_{0.30}]_{0.7}(ZnO)_{0.3}\}_y$ $(Er_2O_3NPs)_{1-y}$, y = 0.005, 0.01, 0.02, 0.03, 0.04 and 0.05. The high purity of chemical powder (99% purity grade) of erbium (III) oxide nanoparticles, Er_2O_3 NPs (Reacton, Alfa Aesar, size of particles = 15 nm), tellurium (IV) oxide, TeO_2(Puratronic, Alfa Aesar), ZnO (Assay, Alfa Aesar) and boron oxide, B_2O_3 (Assay, Alfa Aesar) were commercially obtained and used for sample preparation.

The raw materials were weighted using electrical balance with accuracy of ±0.0001 g. Subsequently, the raw materials were mixed thoroughly and transferred in an alumina crucible. The mixture of raw materials was melted at 900 °C using electrical furnace for 2 h. The choice of melting temperature was done by several times of fabrications with different temperature. It is found that the temperature of 900 °C is the most stable melting temperature to produce high transparency and low fragility of glass materials. The molten was quenched in cylindrical stainless-steel mold. The cylindrical stainless-steel mold containing the glass sample was cooled down at room temperature for 5 h. The glass sample was cut at a thickness of ~2 mm using high precision Isomet Buehler low speed saw machine. The glass sample was polished using sand paper to obtain a smooth surface on both sides. The obtained glass sample is transparent and bubble free. The structural analysis of erbium NPs doped tellurite glass was done by using X-ray diffraction method to confirm the structural arrangement in the glass network. Furthermore, the Mattson 5000 Fourier transform infrared (FTIR) spectrometry at room temperature was conducted to determine the transmission band of each elements in the glass system. The transmission electron microscopy (TEM) technique with the basic principle of the electron microscope was performed to determine the particle size of erbium NPs after the glass formation. Shimadzu-1650PCUV-Vis spectrophotometer was used to analyze the absorption band of the glass sample. The upconversion spectra was measured by using Perkin-Elmer LS 55 Luminescence spectrophotometer.

3. Results and discussion

3.1. X-ray diffraction and transmission electron spectra

As displayed in Fig. 1, the XRD spectra of erbium NPs doped tellurite glass are recorded at room temperature in the range $20^0 \leq \Theta \leq 80°$. The XRD spectra revealed broad diffusion at lower scattering angles suggesting the existence of long-range structural disorder. The presence of broad peaks at around $2\Theta = 30°$ is shown in Fig. 1. The obtained trend is due to the effect of erbium NPs concentration which contribute to the strong XRD broad peaks at 30°. The increasing concentration of erbium NPs results to the narrower of broad peaks. Consequently, the tendency of the glass system to crystallize is increased with increasing amount of erbium NPs. However, the broad peaks obtained from the XRD spectra suggest that erbium NPs doped tellurite glasses are completely amorphous in nature. The size of erbium NPs was determined by using transmission electron microscopy (TEM). TEM analysis was conducted before and after the glass formation to prove the existence of nanoparticles in the glass sample. The images of nanoparticles before and after the glass formation are depicted in Figs. 2a and 2b. It can be seen from Fig. 2a that the size of erbium NPs before the glass formation is ~18 nm, while the size of particles is found increased after the glass formation at ~28 nm as shown in Fig. 2b. The three-dimensional spherical-shape of the particles before and after the glass formation remain unchanged. The increasing size of particles may be subjected to the Oswald ripening effect in which the smaller size of particles is diffused to larger size of particles [17].

3.2. Fourier transform infrared

FTIR spectroscopy is one of the powerful techniques frequently used to analyze the structural parameter of a glass system. Thus, the FTIR

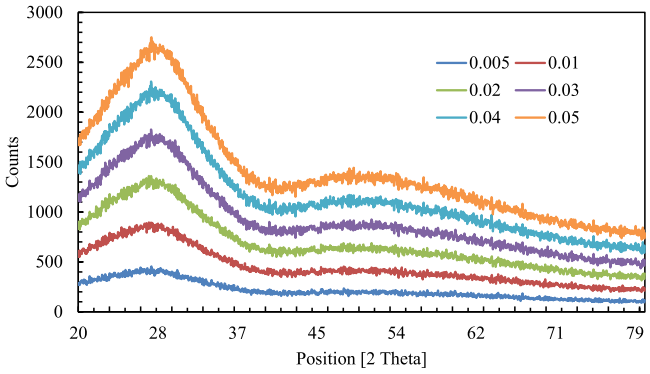

Fig. 1. XRD spectra of erbium NPs doped tellurite glasses.

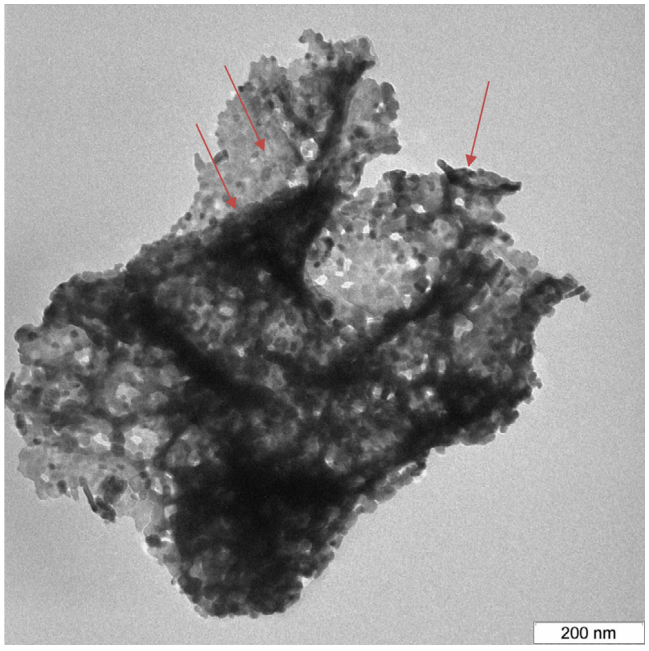

Fig. 2a. TEM image of pure erbium nanoparticles before the glass formation.

spectra of different erbium NPs concentrations are recorded to investigate their internal structure. The transmission spectra of erbium NPs doped tellurite glass are recorded in Fig. 3. It is shown that the erbium NPs doped tellurite glasses consist of several peaks which correspond to the local structure of the glass system. The transmission spectra of erbium NPs doped tellurite glasses consist of three wide absorption bands in the range 656–664 cm^{-1} , 1233–1252 cm^{-1} and 1327–1343 cm^{-1}. In addition, some shoulders are recorded at 414 cm^{-1}– 421 cm^{-1}.

Tellurite oxide consists two types of structural configuration units, i.e., trigonal bipyramid TeO_4 and trigonal pyramid TeO_3 [18]. The presence of transmission band at 656–664 cm^{-1} indicates the information of stretching vibrational modes of Te-O bands in Te-bridging oxygen and Te-nonbridging oxygen respectively. Te-bridging oxygen is attributed to the trigonal bipyramid, TeO_4 structural unit. Meanwhile Te-nonbridging oxygen corresponds to the trigonal pyramid, TeO_3 structural unit. The transmission band in the range of 600–650 cm^{-1}corresponds to the TeO_4 group, and the transmission band in the range of 650–700 cm^{-1} corresponds to the TeO_3 group. Hence, the transmission band shown at 656–664 cm^{-1} in Fig. 3 indicates that the glass system consists of Te-nonbridging oxygen, TeO_3. These bands are broadened with respect to the crystalline TeO_2, which is due to the distribution of bond angles and lengths in the amorphous matrix [19].

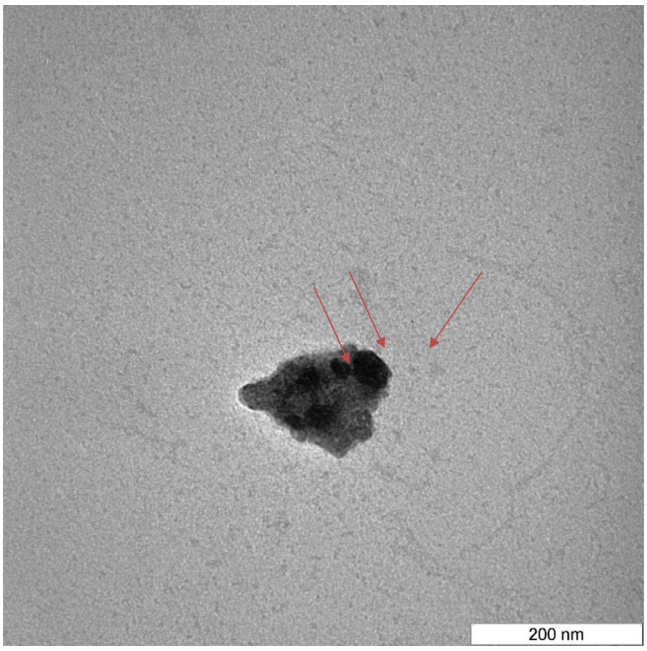

Fig. 2b. TEM image of erbium nanoparticles after the glass formation.

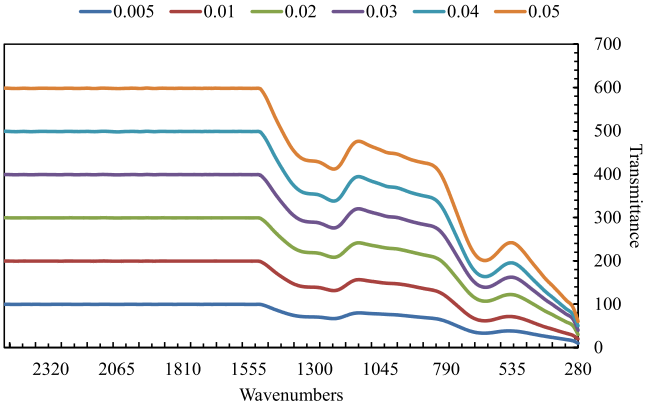

Fig. 3. FTIR spectra of erbium NPs doped tellurite glasses.

The transmission bands of BO_4 and BO_3 are introduced after the glass formation which is due to the substitutions of boroxyl ring. The vibrational modes of borate glass are active in three spectral regions according to the work of Krogh-Moe [20]. The first group of the band around 600–800 cm^{-1} corresponds to the bending vibrations of various borate arrangements B-O-B. The second group of the band located at around 800–1200 cm^{-1} corresponds to the B-O stretching vibrations of tetrahedral BO_4- units. The third region around 1200–1800 cm^{-1} corresponds to the B-O stretching of trigonal BO_3 units. The band spectra observed at 1233–1253 cm^{-1} is due to B-O-B stretching vibrations of polymerized BO_3 groups [21]. The transmission band around 1327–1343 cm^{-1} is associated with the trigonal B-O bond stretching vibrations in isolated trigonal BO_3 units. Moreover, the transmission band at around 1388–1410 cm^{-1} is ascribed to the trigonal B-O bond stretching vibrations of BO_3 units from various types of borate groups. The erbium NPs is not detected by FTIR transmission spectra due to the low concentration.

3.3. Absorption spectra

The optical absorption spectra for the erbium NPs doped tellurite glass are depicted in Fig. 4. It can be seen that the absorption spectra

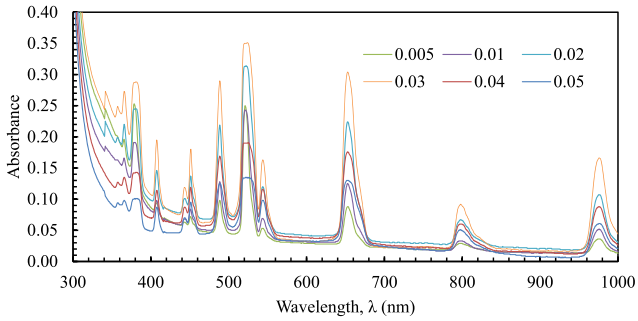

Fig. 4. UV–Vis absorption spectra of erbium NPs doped tellurite glasses.

consist of several sharp peaks indicating the excitation of electrons in 4-f transitions from the ground state, $^4I_{15/2}$ to several excitation levels $^4G_{11/2}$ + $^2H_{9/2}$ + $^4F_{5/2}$ + $^4F_{7/2}$ + $^2H_{11/2}$ + $^4S_{3/2}$ + $^4F_{9/2}$ + $^4I_{9/2}$ + $^4I_{11/2}$ correspond to the excitation energy at 383.5 nm, 408.5 nm, 452.0 nm, 489.0 nm, 525.5 nm, 545.5 nm, 654.5 nm, 800.0 nm and 979.0 nm respectively. The transition levels were confirmed from the previous work of Carnall et al. which study the spectral intensities of the trivalent lanthanides and actinides [22]. It can be seen from the figure that the absorption coefficient decreases with an increase of wavelength. The optical absorption edge is not sharply defined in the present glass samples which are due to their characteristic of amorphous nature [23]. From the figure, it can be seen that the absorption edge is shifted to the longer wavelength with increasing concentration of erbium NPs. Such trend is due to the less rigidity in the glass system [18].

3.4. Extinction coefficient

The extinction coefficient (k) of the glass system is determined by

$$k = \frac{\alpha\lambda}{4\pi}. \quad (1)$$

The value of k is used to calculate the Fermi energy (E_F). The extinction coefficient obeys Fermi–Dirac distribution function for all glass samples.

$$k(\lambda) = \frac{1}{1 + \exp(\frac{E - E_F}{K_B T})} \quad (2)$$

where E is the photon energy, E_F represents Fermi energy, K_B is the Boltzmann constant and T is the temperature. The plotted graph of extinction coefficient of the glass series is shown in Fig. 5. It can be seen from the figure that the extinction coefficient, k for the glass series decreases with an increase in wavelength. This trend is due to the decreasing value of absorption coefficient with increasing wavelength. It is known that the extinction coefficient, k depends on the wavelength of light propagation through the materials. Hence, the change of wavelength may result in the change of extinction coefficient.

The obtained values of Fermi energy for the two glass series are tabulated in Table 1. It can be observed from the table that the value of Fermi energy decreases with increasing amount of erbium NPs. This result indicates that the glass system tends to be more conductive with increasing quantity of the erbium NPs. The addition of Er^{3+} ions in the glass matrix leads to the increasing number of BO_4^- units. The higher number of BO_4^- units will cause to the decrease in the degree of delocalization of electrons which increases donor centers in the glass matrix [24]. Thus, the Fermi energy is decreased. The higher value of Fermi energy than k_BT indicates the insulation nature of the materials.

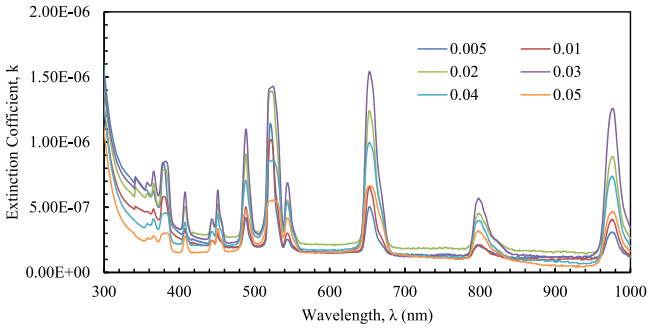

Fig. 5. Extinction coefficient versus wavelength of erbium NPs doped zinc tellurite glasses.

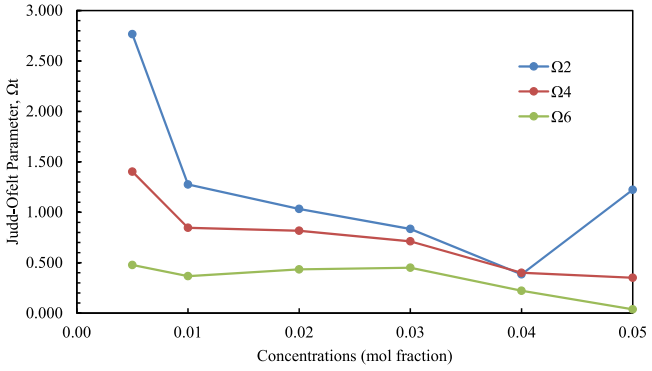

Fig. 6. Judd–ofelt parameter, $\Omega_t (t = 2, 4, 6)$ versus concentrations of erbium NPs doped zinc tellurite glasses.

Table 1
Fermi Energy of erbium NPs doped tellurite glasses.

Mol fraction	Fermi Energy, E_F (eV)
Erbium nanoparticles	
0.005	4.414
0.01	4.390
0.02	4.372
0.03	4.366
0.04	4.308
0.05	4.304

3.5. Judd-Ofelt analysis

The theoretical estimation of spectroscopic and laser parameters of erbium NPs doped tellurite glass can be investigated by way of Judd–Ofelt (J–O) theory from the absorption spectra. The calculation method to compute J–O theory can be found in previous research [25,26]. Hence, we only focus on the results of spectral parameters. J–O theory provides information of spectral parameters, Ω_t(t = 2, 4, 6), oscillation strength, radiative transitions within $4f^n$ configuration and emission lifetime. The validity of results and reliable calculations have been obtained by comparing the experimental and calculated line strength and oscillation strength which are listed in Table 2. Based on the least-square fitting method, the spectral parameters Ω_t (t = 2, 4, 6) of erbium NPs doped tellurite glass have been obtained and listed in Table 3. The trend of spectral parameters along with erbium NPs concentration is depicted in Fig. 6.

It has been established that the Ω_2 and Ω_4 parameters are strongly affected by the local environment of erbium ions, Er^{3+}. Moreover, the values of Ω_2 and Ω_4 parameters correspond to the symmetry and polarization of local structure and the bonds of Er^{3+} to the ligands. It can be seen from Fig. 6 that the Ω_2 parameter is higher at 0.005 mol fraction of erbium NPs which indicates the high polarization of Er^{3+} ions and asymmetry around Er^{3+} [27]. Moreover, the maximum point of Er^{3+} NPs ions at 0.005 is due to the large polarization of Te^{4+} and asymmetry of tellurite glasses (Jlassi et al. 2011). Hence, the chemical bonds of Er^{3+} possess strong covalency at 0.005 mol fraction. The growing covalency of materials will increase the value of optical band gap which is due to the lower ionicity of materials [28]. Moreover, the effect of covalency between the Er^{3+} ions and ligand bonds will reduce the electron donor power and result to the decreasing value of optical basicity.

Fig. 6 shows that the value of Ω_2 parameter starts to decrease with an increase of erbium NPs concentration. Such trend indicates that the covalency of Er^{3+} decreases and the reduction of asymmetry around Er^{3+}. The reduction of covalency in Er^{3+} ions to the ligands is related to the degree of rigidity which reflect the amorphous nature in the glass system [29]. Decrease in covalency indicates an increase of electron donor power which leads to the decrease of optical band gap and optical basicity. This trend corresponds to the previous value of optical band gap which decreases along with erbium NPs concentration. However, at 0.05 mol fraction of erbium NPs, the Ω_2 parameter increases. This trend is due to the nephelauxetic effect and a shift of the barycenter of the absorption bands along with erbium NPs concentration [30].

Ω_6 parameter is not dependent on the Er^{3+} local environment but related to the rigidity of Er^{3+} ions bonds to the ligand. Moreover, the Ω_6 parameter is ascribed to the overlap integrals of 4f and 5d orbits [31]. The non-linear trend is found in Ω_6 parameter as shown in Fig. 6. It can be seen that the lowest point of Ω_6 parameter is at 0.05 mol fraction which indicates the reduction of rigidity of Er^{3+} ions to the ligand. The reduction of Ω_6 parameter can be explained by comparing the value of electronegativity between cations and anions in the glass system. Since the values of electronegativity, for B, Te, Zn, O and Er atoms are **2.04, 2.10, 1.65, 3.44 and 1.24** respectively, the Er-O bond is found weaker among the other atoms which leads to the reduction of Ω_6 parameter [32]. It can be seen from Fig. 5 that the Ω_6 parameter is slightly increased from 0.01 mol fraction to the highest 0.03 mol fraction. Such trend indicates that the stark splitting of energy levels is increased within 0.01–0.03 mol fraction which leads to the widen of emission band. Moreover, the enhancement of Ω_6 parameter is most probably due to the increasing ionicity and vibrational amplitude of Er-O bond.

The radiative properties of erbium NPs doped tellurite glass are calculated and tabulated in Table 4. The strongest radiative probability, A_{rad} for the glass sample is located at Er^{3+}: $^2H_{11/2} \longrightarrow {}^4I_{15/2}$ transition which indicates strong green emission. Furthermore, the branching ratio, β value at Er^{3+}: $^2H_{11/2} \longrightarrow {}^4I_{15/2}$ transition is 0.963 which suggests high possibility of laser application in the glass sample. The lifetime of the estimated emission is found at 0.322 ms which is lower than the other transitions. Decrease in radiative lifetime is due to the increase of non-radiative decay. Moreover, the decrease in particle–particle distance results in the enhancement of inter-coupling and decay channels which in turn decrease the lifetime [33]. Meanwhile, the longer of a lifetime at the transition of $^4I_{13/2}$ level gives an advantage to the population inversion between the $^4I_{13/2}$ and $^4I_{15/2}$ levels [34]. It is observed that the lifetime of erbium NPs doped tellurite glass is greater at $^4I_{11/2} \rightarrow {}^4I_{15/2}$ transition level.

3.6. Upconversion spectra

The inset of Fig. 7 shows the upconversion emission band under excitation of 800 nm. The selection of excitation level is done by using the previous data of absorption spectra which locates the excitation level at 800 nm. It can be seen from the figure that the upconversion emission band is observed at 390 nm which correspond to $^2H_{9/2} \rightarrow {}^4I_{15/2}$ transition. The Russell–Saunders coupling explained that the observed emission peak is mainly due to the deviation of 4f configuration [35–39]. Thus, the emission at ultraviolet and infrared region can be

Table 2
Dipole line strengths S, oscillator strength, f and calculated JO intensity parameters of erbium NPs doped zinc tellurite glasses.

Transition	Wavelength	Line strength, S($\times 10^{-20}$cm^2)		Oscillator strengths, f ($\times 10^{-20}$cm^2)	
(from $^4I_{15/2}$)	λ (nm)	Measured, S_{meas}	Calculated, S_{calc}	Measured, f_{meas}	Calculated, f_{calc}
Erbium nanoparticles (0.05 mol fraction)					
$^4F_{5/2}$	448	0.051	0.051	0.144	0.144
$^4F_{7/2}$	482	0.108	0.066	0.285	0.173
$^4H_{11/2}$	515	0.191	0.202	0.473	0.500
$^4S_{3/2}$	647	0.180	1.037	0.354	2.039
$^4F_{9/2}$	800	0.061	0.075	0.096	0.119
$^2I_{9/2}$	960	0.069	0.008	0.091	0.011

Table 3
JO intensity parameters Ω_t = (t = 2, 4, 6) of erbium NPs doped tellurite glasses.

Mol fraction	Judd–ofelt parameters, Ω_t ($\times 10^{-21}$ cm^2)		
	$\Omega 2$	$\Omega 4$	$\Omega 6$
Erbium nanoparticles			
0.005	2.766	1.403	0.478
0.01	1.276	0.847	0.367
0.02	1.033	0.817	0.434
0.03	0.835	0.712	0.450
0.04	0.384	0.400	0.222
0.05	1.223	0.351	0.037

Table 4
Calculated transition probabilities and branching ratio of erbium nanoparticles doped zinc borotellurite glasses (0.05 mol fraction)

Transitions			λ (nm)	A_{MD} (s^{-1})	A_{ED} (s^{-1})	β	Lifetime, t (ms)
$^4I_{13/2}$	→	$^4I_{15/2}$	1530	64.75	11.768	1.000	13.070
$^4I_{11/2}$	→	$^4I_{13/2}$	2804	14.66	3.069	0.443	
		$^4I_{15/2}$	990		22.252	0.557	25.014
$^4I_{9/2}$	→	$^4I_{11/2}$	4168	2.25	0.189	0.037	
		$^4I_{13/2}$	1676		3.366	0.051	
		$^4I_{15/2}$	800		60.260	0.912	15.136
$^4F_{9/2}$	→	$^4I_{9/2}$	3771	4.92	1.714	0.016	
		$^4I_{11/2}$	1980	11.82	8.910	0.049	
		$^4I_{13/2}$	1161		23.382	0.056	
		$^4I_{15/2}$	660		368.654	0.879	2.384
$^4S_{3/2}$	→	$^4I_{9/2}$	1710		9.267	0.090	
		$^4I_{11/2}$	1212		2.832	0.027	
		$^4I_{13/2}$	846		26.955	0.261	
		$^4I_{15/2}$	545		64.169	0.622	9.688
$^2H_{11/2}$	→	$^4F_{9/2}$	2497		10.636	0.003	
		$^4I_{9/2}$	1502		34.765	0.011	
		$^4I_{11/2}$	1104		27.394	0.009	
		$^4I_{13/2}$	792		43.258	0.014	
		$^4I_{15/2}$	522		2986.464	0.963	0.322
$^4F_{7/2}$	→	$^4F_{9/2}$	1942		2.361	0.003	
		$^4I_{9/2}$	1282		21.784	0.031	
		$^4I_{11/2}$	980		68.673	0.099	
		$^4I_{13/2}$	726		201.146	0.289	
		$^4I_{15/2}$	493		402.700	0.578	1.435
$^2G_{9/2}$	→	$^4F_{7/2}$	2439		4.569	0.007	
		$^2H_{11/2}$	1907		7.718	0.011	
		$^4F_{9/2}$	1081		7.268	0.010	
		$^4I_{9/2}$	840		17.147	0.024	
		$^4I_{11/2}$	699		121.869	0.174	
		$^4I_{13/2}$	560		432.970	0.617	
		$^4I_{15/2}$	410		110.247	0.157	1.425

observed from the excitation of Er^{3+} ions. It can be seen from the figure that erbium NPs doped tellurite glass possesses an intense emission peak at 0.05 mol fraction. The intense emission peak is due to the high amount of excited Er^{3+} nanoparticles ions at 0.05 mol fraction.

Fig. 8 shows a schematic diagram of upconversion emission mechanisms for erbium NPs doped tellurite glass. The Er^{3+} ions at the ground

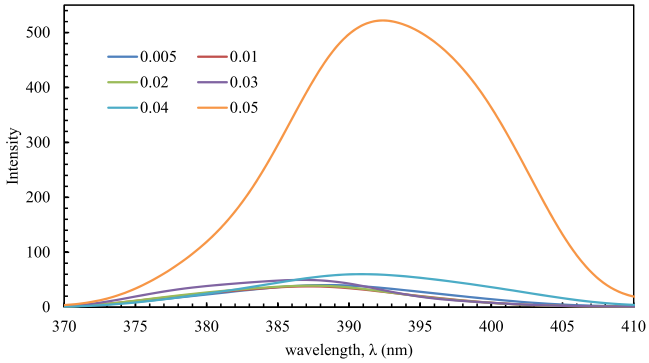

Fig. 7. Upconversion emission spectra of erbium nanoparticles doped zinc borotellurite glasses.

state level, $^4I_{15/2}$ are excited by using 800 nm of wavelength to the upper level at $^4I_{9/2}$. The ions at $^4I_{9/2}$ are then promoted to $^4G_{11/2}$ through excitation absorption process (ESA):

$$^4I_{9/2} + \text{a photon} \rightarrow {}^4G_{11/2}$$

The energy transfer (ET) process is also produced to populate the excited states:

$$^4I_{9/2} + {}^4I_{9/2} \rightarrow {}^4G_{11/2} + {}^4I_{15/2}$$

The ions at $^4G_{11/2}$ are decay nonradiatively through nonradiative relaxation (NR) process to populate $^2H_{9/2}$ level. The upconverted violet emission is produced by radiative relaxation process at $^2H_{9/2}$ (390 nm) level to the ground state, $^4I_{15/2}$ level. The enhancement of emission peak at 0.05 mol fraction of erbium nanoparticles is due to the energy transfer process:

$$^4G_{11/2} + {}^4F_{7/2} \rightarrow {}^2H_{9/2} + {}^2H_{9/2}$$

The red shift as shown in Fig. 7 is due to the presence of impurity band generated from the doping concentrations. Another possibility is that, the red shift is due to the potential fluctuations that leads to the formation of vacancies, impurities, dangling bonds and structural defects [40]. Meanwhile, the blue shift of the emission peaks is usually related to the quantum confinement effects in nanoparticles. The strong quantum confinement leads to the increasing number of free charge carriers and oscillator strength of the glass system.

4. Conclusions

In conclusions, the erbium NPs doped tellurite glasses were successfully fabricated via melt-quenched technique and characterized its optical properties. The structural analysis was performed based on the XRD, FTIR and TEM analysis which confirmed its amorphous nature, the formation of nonbridging oxygen and the existence of nanoparticles (~28 nm). The spectral analysis of erbium NPs doped tellurite glass was carried out based on UV-Vis spectroscopy, upconversion spectra and it is found that the erbium NPs doped tellurite glass possesses: several

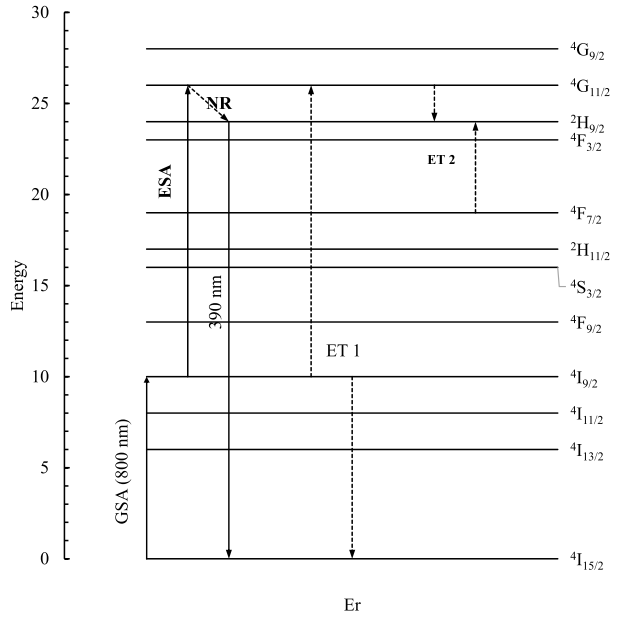

Fig. 8. Schematic diagram of erbium NPs doped tellurite glasses for upconversion emission.

excitation levels at $^4G_{11/2}$ + $^2H_{9/2}$ + $^4F_{5/2}$ + $^4F_{7/2}$ + $^2H_{11/2}$ + $^4S_{3/2}$ + $^4F_{9/2}$ + $^4I_{9/2}$ + $^4I_{11/2}$ which is further analyzed to determine the spectral parameters. The spectral parameters were shown to follow the trend of $\Omega_2 > \Omega_4 > \Omega_6$. Based on the radiative probability, A_{rad} and branching ratio, β, it is suggested that the erbium NPs doped tellurite glass has strong green emission (Er^{3+}: $^2H_{11/2} \longrightarrow {}^4I_{15/2}$) and high possibility of green laser application. The upconversion emission excited at 800 nm shows emission at ultraviolet region (390 nm) which is beneficial to the production of ultraviolet lasers. Based on these results, the proposed materials are suitable materials for laser applications due to their outstanding optical performance.

Acknowledgments

This research was financially supported by Geran Penyelidikan Universiti (GPU), Malaysia, Sultan Idris Education University, Malaysia (Grant code: 2018-0139-103-01) and Skim Geran Penyelidikan Fundamental (FRGS), Malaysia Fasa 1/2018 (Grant code: 2019-0006-102-02). The authors would like to thank the following institutions for equipment support: Faculty of Science and Mathematics, Universiti Pendidikan Sultan Idris and Faculty of Science, Universiti Putra Malaysia.

References

[1] M.N. Azlan, M.K. Halimah, Role of Nd^{3+} nanoparticles on enhanced optical efficiency in borotellurite glass for optical fiber, Results Phys. 11 (2018) 58–64.
[2] A. Gonçalves, V.S. Zanuto, G.A.S. Flizikowski, A.N. Medina, F.L. Hegeto, A. Somer, J.L. Gomes Jr., J.V. Gunha, G.K. Cruz, C. Jacinto, N.G.C. Astrath, A. Novatski, Luminescence and upconversion processes in Er^{3+}–doped tellurite glasses, J. Lumin. 201 (2018) 110–114.
[3] Jirapan Dutchaneephet, Apichart Limpichaipanit, Athipong Ngamjarurojana, Optical spectroscopic investigations of neodymium and erbium added bismuth silicate glasses, Optik 178 (2019) 111–116.
[4] M. Azam, V.K. Rai, Enhanced frequency upconversion in Er3+-Yb3+ codoped heavy metal oxides based tellurite glasses, Methods Appl. Flourescence 6 (2) (2018) 025002.
[5] M. Azam, V.K. Rai, Ho3+-Yb3+ Codoped tellurite based glass in visible lasers and optical devices: Judd-Ofelt analysis and frequency upconversion, Solid State Sci. 6 (2017) 7-5.
[6] M. Azam, V.K. Rai, P. Mishra, Enhanced frequency upconversion and non-colour tunability in Er3+-Yb3+ codoped TeO2-WO3-Pb3O4 glasses, J. Mater. Sci., Mater. Electron. 27 (2016) 12633–12641.
[7] M. Azam, V.K. Rai, D.K. Mohanty, Spectroscopy and enhanced frequency up-conversion in Nd3+-Yb3+ codoped TPO glasses: energy transfer and NIR visible upconverter, Methods Appl. Flourescence 5 (3) (2017) 035005.
[8] R. El-Mallawany, Longitudinal elastic constants of tellurite glasse, J. Appl. Phys. 73 (10) (1993) 4878–4880.
[9] R.A. El-Mallawany, G.A. Saunders, Elastic behaviour under pressure of the binary tellurite glasses TeO_2-$ZnCl_2$ and TeO_2-WO_3, J. Mater. Sci. Lett. 6 (1987) 443–446.
[10] N. Sooraj Hussain, G. Hungerford, R. El-Mallawany, M.J.M. Gomes, M.A. Lopes, Nasar Ali, J.D. Santos, S. Buddhudu, Absorption and emission analysis of RE^{3+}(Sm^{3+} and Dy^{3+}): Lithium Boro Tellurite Glasses.., J. Nanosci. Nanotechnol. 9 (2009) 3672–3677.
[11] R. El-Mallawany, Specific heat capacity of semiconducting glasses: Binary vanadium tellurite, Phys. Status Solidi a 177 (2) (2000) 439–444.
[12] R.A. El-Mallawany, L.M. Sharaf El-Deen, M.M. Elkholy, Dielectric properties and polarizability of molybdenum tellurite glasses, J. Mater. Sci. 31 (1996) 6339–6343.
[13] I.Z. Hager, R. El-Mallawany, M. Poulain, Infrared and Raman spectra of new molybdenum and tungsten oxyfluoride glasses, J. Mater. Sci. 34 (1999) 5163–5168.
[14] S. Peng, L. Wu, B. Wang, F. Yang, Y. Qi, Y. Zhou, Intense visible upconversion and energy transfer in Ho^{3+}/Yb^{3+} codoped tellurite glasses for potential fiber laser, Opt. Fiber Technol. 22 (2015) 95–101.
[15] A.S. Mahraz, M.R. Sahar, S.K. Ghoshal, M. Reza Dousti, Concentration dependent luminescence quenching of Er^{3+}-doped zinc boro-tellurite glass, J. Lumin. 144 (2013) 139–145.
[16] Maximilian Heinz, Vasiliy V. Srabionyan, Leon A. Avakyan, Aram L. Bugaev, Anna V. Skidanenko, Sviatoslav Yu Kaptelinin, Jürgen Ihlemann, Jörg Meinertz, Christian Patzig, Manfred Dubiel, Lusegen A. Bugaev, Formation of bimetallic gold-silver nanoparticles in glass by UV laser irradiation, J. Alloys Compd. 767 (2018) 1253–1263.
[17] N.N. Yusof, S.K. Ghoshal, M.N. Azlan, Optical properties of titania nanoparticles embedded Er^{3+} -doped tellurite glass: Judd-Ofelt analysis, J. Alloys Compd. 724 (2017) 1083–1092.
[18] P. Gayathri, K. Sadhana, Mouli V. Chandra, Optical, physical and structural studies of boro-zinc tellurite glasses, Physica B 406 (2011) 1242–1247.
[19] R. Dousti, M. Sahar, S. Ghoshal, Effect of agcl on spectroscopic properties of erbium doped zinc tellurite glass, J. Mol. Struct. 1035 (2013) 6–12.
[20] C. Juien, M. Massot, M. Balkanski, Infrared studies of the structure of borate glasses, Mater. Sci. Eng. 3 (1989) 307–312.
[21] X.A. Shen, T.F. Xu, X.D. Zhang, S.X. Dai, Q.H. Nie, X.H. Zhang, Effect of SiO_2 content on the thermal stability and spectroscopic properties of Er^{3+}/Yb^{3+} co-doped tellurite borate glasses, Physica B 389 (2) (2007) 242–247.
[22] W.T. Carnall, P.R. Fields, K. Rajnak, Spectral intensities of the trivalent lanthanides and actinides in solution. II. Pm3+, Sm3+, Eu3+, Gd3+, Tb3+, Dy3+, and Ho3+, J. Chem. Phys. 49 (1968) article 4424.
[23] K.V. Raju, C.N. Raju, S. Sailaja, B.S. Reddy, Judd–Ofelt analysis and photoluminescence properties of RE^{3+}(RE = & Nd): Cadmium lithium boro tellurite glasses, Solid State Sci. 15 (2013) 102–109.
[24] D. Ramteke, R.S. Gedam, Luminescence properties of Gd3+ containing glasses for ultra-violet (UV) light, J. Rare Earths 32 (2014) 389–393.
[25] A.M. Hamza, M.K. Halimah, F.D. Muhammad, K.T. Chan, Physical properties, ligand field and Judd-Ofelt intensity parameters of bio-silicate borotellurite glass system doped with erbium oxide, J. Lumin. 207 (2019) 497–506.
[26] N. Elkhoshkhany, Samir Y. Marzouk, Mohamed A. Khattab, Shaimaa A. Dessouki, Influence of Sm2O3 addition on Judd-Ofelt parameters, thermal and optical properties of the TeO2-Li2O-ZnO-Nb2O5 glass system, Mater. Charact. 144 (2018) 274–286.
[27] Nur Liyana Amiar Rodin, M.R. Sahar, Erbium doped sodium magnesium borotellurite glass: Stability and Judd-Ofelt analysis, Mater. Chem. Phys. 216 (2018) 177–185.
[28] R. Lachheb, A. Herrmann, A.A. Assadi, J. Reiter, J. Körner, J. Hein, C. Rüssel, R. Maâlej, K. Damak, Judd–Ofelt analysis and experimental spectroscopic study of erbium doped phosphate glasses, J. Lumin. 201 (2018) 245–254.
[29] F. Ahmadi, R. Hussin, S.K. Ghoshal, Judd-Ofelt intensity parameters of samarium-doped magnesium zinc sulfophosphate glass, J. Non-Crystall. Solids 448 (2016) 43–51.
[30] Y. Fang, Hu Lili, Liao Meisong, Wen Lei, Effect of bismuth oxide on the thermal stability and Judd–Ofelt parameters of Er^{3+}/Yb^{3+} co-doped aluminophosphate glasses, Spectrochim. Acta A 68 (2007) 542–547.
[31] Muzhi Cai, Beier Zhou, Fengchao Wang, Tao Wei, Ying Tian, Jiajia Zhou, Shiqing Xu, Junjie Zhang, R2O3 (R = La, Y) modified erbium activated germanate glasses for mid-infrared 2.7 μm laser materials, Sci. Rep. 5 (2015) Article number: 13056.
[32] J.E. Stanworth, Tellurite glasses, Nature 169 (4301) (1952) 581–582.
[33] Zhousu Xu, Jinhua Yan, Cheng Xu, Cheng Cheng, Chun Jiang, Xiaofeng Liu, Jianrong Qiu, Tunable near-infrared emission and fluorescent lifetime of PbSe quantum dot-doped borosilicate glass, J. Alloys Compd. 711 (2017) 58–63.

[34] D. Yin, Qi Yawei, Peng Shengxi, Zheng Shichao, Chen Fen, Yang Gaobo, Wang Xunsi, Zhou Yaxun, Er^{3+}/Tm^{3+} codoped tellurite glass for blue upconversion—Structure, thermal stability and spectroscopic properties, J. Lumin. 146 (2014) 141–149.

[35] Pan Cheng, Yaxun Zhou, Minghan Zhou, Xiue Su, Zizhong Zhou, Gaobo Yang, Enhanced broadband near-infrared luminescence from Pr^{3+} -doped tellurite glass with silver nanoparticles, Opt. Mater. 73 (2017) 102–110.

[36] T. Zuo, Z. Sun, Y. Zhao, X. Jiang, X. Gao, The big red shift of photoluminescence of Mn dopants in strained CdS: A case study of Mn-doped MnS-CdS heteronanostructures, J. Am. Chem. Soc. 132 (2010) 6618–6619.

[37] Ren Xiaozhi Liu, Ke Zhang, Peng Zhang, Feng Teng, Zhenxing Zhang, Erqing Xie, Pengxun Yan, Green photoluminescence from erbium-doped molybdenum trioxide, Mater. Lett. 122 (2014) 320–322.

[38] Mahraz S. Ashur, M.R. Sahar, S.K. Ghoshal, Enhanced luminescence from silver nanoparticles integrated Er^{3+}-doped boro-tellurite glasses: Impact of annealing temperature, J. Alloys Compd. 649 (2015) 1102–1109.

[39] K.V. Raju, C.N. Raju, S. Sailaja, B.S. Reddy, Judd–Ofelt analysis and photoluminescence properties of RE^{3+} (RE = Er & Nd): Cadmium lithium boro tellurite glasses, Solid State Sci. 15 (2013) 102–109.

[40] Ahmed Ben Slimane, Adel Najar, Rami Elafandy, Damián San-Román-Alerigi, Dalaver Anjum, Tien Khee Ng, Boon S Ooi, On the phenomenon of large photoluminescence red shift in GaN nanoparticles, Nanoscale Res. Lett. 8 (2013) 342.